Materials Today Energy 44 (2024) 101646

Contents lists available at ScienceDirect

Materials Today Energy

journal homepage: www.journals.elsevier.com/materials-today-energy/

Sustainable luminescent solar concentrators with superior photodegradation resistance employing heptagon-embedded polycyclic aromatic dicarboximides as emitters

Alberto Picchi [a], Kritchasorn Kantarod [b], Massimo Ilarioni [c], Marco Carlotti [a, **], Pawaret Leowanawat [b], Andrea Pucci [a, *]

[a] Dipartimento di Chimica e Chimica Industriale, Università di Pisa, Via Moruzzi 13, 56124, Pisa, Italy
[b] Center of Excellence for Innovation in Chemistry (PERCH-CIC) and Department of Chemistry, Faculty of Science, Mahidol University, Bangkok, 10400, Thailand
[c] I&S srl, Via F.lli Chiaruffi, 12, 50067, Rignano sull'Arno, Firenze, Italy

ARTICLE INFO

Article history:
Received 30 April 2024
Received in revised form
25 June 2024
Accepted 9 July 2024
Available online 14 July 2024

Keywords:
LSC
PMMA
Fluorophore
Solar harvesting
Chemical recycling
Circular economy

ABSTRACT

Luminescent Solar Concentrators (LSCs) are a type of light concentrating devices which offer several advantages over other optical methods, like the possibility of working with diffuse light and the appealing aesthetics, which makes them an ideal technology for their integration in building's facades of urban settings. In order to improve their effectiveness and foster a large-scale adoption, solutions to lower the impact of their production and extend their lifetime would be extremely beneficial. Photostability is crucial for fluorophores used in LSCs, as they have to endure extended sunlight exposure over years. UV radiation can alter the structure of organic emitters, reducing LSC efficiency and causing panel replacement, with economic costs and environmental implications. In this study, two push-pull dyes comprising distorted heptagonal inclusions—namely, Peri2F and Nap2Car—were investigated as emitters for bulk PMMA-based LSCs fabricated employing chemically regenerated monomers (r-MMA). Compared to the use of virgin monomer, the Global Warming Potential of slab production is about four times smaller, thereby enhancing the sustainability and encouraging circularity of large-scale LSC fabrication. The most effective Peri2F/r-PMMA system yielded an η_{dev} of 0.7%, lower than that of devices comprising the state-of-the-art emitter LR305. Remarkably, however, Peri2F showed a far superior resistance to photodegradation. Forecast analysis estimated that the LSC containing 100 ppm of Peri2F can match LR305 performance in r-PMMA after about 1 year of use, with less than 2% decrease in initial emission intensity.

1. Introduction

Due to their low price and high compatibility with polymeric materials, organic fluorophores are among the preferred options for harvesting sunlight photons, which makes them useful for energy applications [1]. Depending on their sector of use, the molecular structures of organic fluorophores can be tuned to combine their light-harvesting characteristics with the necessary phase dispersion within the selected polymer matrix. In this way, their color and appearance can be controlled, making them easily integrated into solar energy technologies, e.g. building-integrated photovoltaics (BIPV) [2,3]. An example of these consists of Luminescent Solar Concentrators (LSCs), devices composed of a slab of polymeric or glassy material doped with fluorophore molecules, which absorb incident radiation and re-emit it, directing the photons towards the edges, thus resulting in light concentration (Fig. 1b) [4]. The resulting higher flux of photons can easily be exploited by small-area photovoltaic cells placed on the device's edges. To allow for high light concentration efficiencies, high photoluminescence quantum yields (PLQYs) and large Stokes shifts are required [5,6]. Furthermore, aggregation-caused quenching (ACQ) must be prevented due to its detrimental effect on the emission and device efficiencies [7].

* Corresponding author.
** Corresponding author.
E-mail addresses: marco.carlotti@unipi.it (M. Carlotti), andrea.pucci@unipi.it (A. Pucci).

https://doi.org/10.1016/j.mtener.2024.101646

Abbreviations

ACQ	Aggregation-caused quenching
AIBN	Azobisisobutyronitrile
BIPV	Building-integrated photovoltaics
BODIPY	Boron dipyrromethene
HOMO	Highest occupied molecular orbital
LSC	Luminescent solar concentrator
LUMO	Lowest unoccupied molecular orbital
MMA	Methyl methacrylate
OPV	Organic photovoltaic cell
PADI	Polycyclic aromatic dicarboximides
PLQY	Photoluminescence quantum yield
PMMA	Poly(methyl methacrylate)
PV	Photovoltaic
PVC	Poly(vinyl chloride)
r-MMA	Regenerated methyl methacrylate
r-PMMA	Recycled poly(methyl methacrylate)
UV	Ultraviolet

Photostability is a critical trait for fluorophores used in LSC applications, as these molecules must endure prolonged exposure to sunlight, which includes UV radiation, often spanning years. The literature extensively details the effects of energetic radiation organic dyes [8]. When subjected to UV photons, organic emitters may experience structural alterations, thus resulting in fluorescence losses. Notwithstanding that organic dyes improve photostability by two orders of magnitude when trapped in solid matrices [9], such processes still remain detrimental for LSC efficiency, thus possibly requiring its replacement. This incurs economic costs and environmental consequences, including increased waste production and energy consumption associated with manufacturing and installing new panels., For example, El-Bashir et al. demonstrated that the relative absorption of a coumarin fluorophore, i.e. Macrolex Fluorescent Red G, embedded in poly(-methyl methacrylate) (PMMA), decreased by approximately 8% after one year of sunlight exposure in Riyad, Saudi Arabia [10]. Also, Mooney et al. [11] observed that only one of the three investigated BODIPY derivatives had discrete photostability with about 40% relative absorption drop over 700 simulated hours of thermally accelerated UV aging. Recently, an LSC based on tetra(t-Butyl) rubrene and a thiol-ene resin was reported to show a long lifetime by Zhang et al. [12], with no efficiency loss after 800 h of UV irradiation. However, the radiation power was relatively low, i.e., 2.8 W/m^2, if compared to the other examples reported herein (see Table S1). Kinderman et al. [13] measured for F570 and F083 Lumogen dyes dispersed in acrylic LSC plates a relative absorption reduction of 38 and 31%, respectively, after the equivalent of 8 months of outdoor exposure in West Europe. Earp et al. [14] reported a 50% decrease in emission after 14 days of sunlight irradiation for the same Lumogen F083 in PMMA, whereas the relative absorption decreased by 9%, indicating that even a slight reduction in absorbance can result in significant output losses. Among the dyes of the Lumogen series, the F Red 305 (LR305) is considered as the state of the art in LSC, thanks to its broad absorption and PLQY close to unity [15–18]. Because of its relevance, also its photostability has been extensively investigated in the literature, both experimentally and from a mechanistic perspective [19]. For example, in the work of Hyldahl et al. [20], the absorption maximum of a LR305 LSC panel decreased by around 5% after around 600 h of solar irradiation (95 mW/cm^2). Li et al. [21] showed that the performance of an OPV-LSC system containing LR305 decreased by about 20% after 300 h of continuous 1 Sun illumination. Delgado et al. [22] observed a 7% efficiency drop in LSC prototypes containing LR305 after 4 months of outdoor exposure. The same fluorophore in a fluoropolymer lost 13% efficiency after 800 h UV irradiation (50 W/m^2), as reported by Pintossi et al. [23]. It must be noted that the fluorophore lifetime is directly affected by the polymer matrix, and some results from the literature might not be comparable [24]. This is because LR305 photodegradation, as well as that of most organic dyes, involves the homolytic cleavage of carbon-heteroatom bonds that result in the formation of stabilized radicals [25]. Such degradation pathways, albeit less impactful than other kinds of fluorophores, can still become significant when light irradiation is extended to longer periods of time despite the remarkable performances of LR305. The development of efficient emitters less prone to photodegradation could prolong the lifetime of assembled LSC devices, making such technology more affordable and sustainable. In this regard, compounds characterized by the absence of moieties easily cleavable by homolytic scissions could offer a superior resistance to photodegradation.

Inspired by the work of Kantarod et al. [26], who synthesized a series of heptagon-embedded push-pull molecules showing high quantum yields (up to 90%) and small HOMO-LUMO energy gaps for a more efficient solar harvesting, we prepared LSC slabs based on two of the most efficient compounds reported therein. The first selected fluorophore, shown in Fig. 1a and named *Nap2Car*, consists of push-pull molecule where a naphthalene dicarboximide acts as acceptor moiety and a dibenzo-heptagon bearing two carbazole substituents act as donor. The second fluorophore, which we will refer to as *Peri2F* (Fig. 1a and Fig. S1b), differs from the former as it

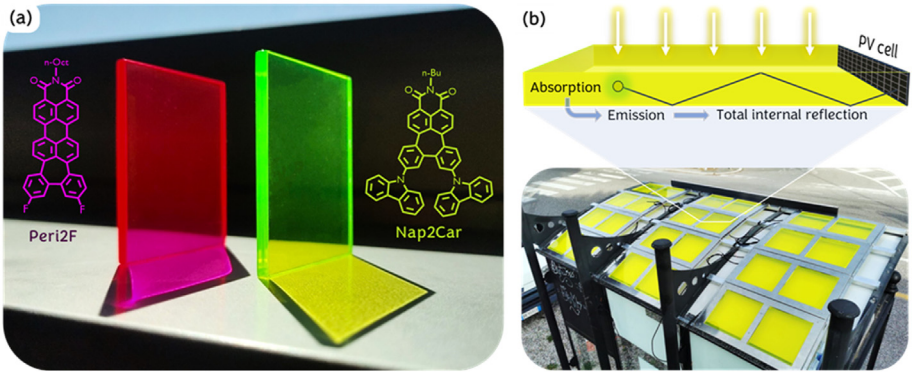

Fig. 1. (a) Peri2F (left) and Nap2Car (right) molecular structures and LSC appearances; (b) Illustration of LSC functioning from a photograph taken during LSC installation on a bus shelter in Livorno, Italy.

presents a perylene dicarboximide core containing a heptagonal ring and two fluoride substituents in the di-benzoheptagon donor moiety. Compared to the former, the latter does present bonds that can yield to the ready formation of stable radicals from a homolytic cleavage. The introduction of a seven-membered ring gives a curved shape to the molecule, hindering aggregation and fixing the geometry of the molecule, thus contributing to the high quantum yield observed.

As host material, we selected PMMA, a widely used commodity plastic for its transparency and high internal transmittance, i.e., key features that allow photons to penetrate the material and be conveyed to the edges [27,28]. Taking into consideration the overall sustainability of the LSC production process, PMMA was synthesized by using a high-purity chemically regenerated methyl methacrylate (r-MMA), so we will refer to it in this paper as r-PMMA. The properties of r-PMMA for LSC applications have been recently described by our research group [29]. r-PMMA has been shown to be a sustainable alternative to synthetically derived PMMA, as the environmental impact of its production is reduced by 75%. Furthermore, its use does not adversely affect the LSC performance but slightly increases the photodegradation rate if impurities are present. When considering a future semi-industrial production of PMMA sheets, leading to materials totally composed of plastics, the use and recycle of r-PMMA would ensure a circular economy approach, the efficacy of which could indeed benefit from the use of fluorophores which are particularly resistant to photodegradation.

Notably, in this study, we prepared r-PMMA-based LSCs employing a free-radical bulk polymerization *via* a cell casting process. For each fluorophore (*Nap2Car* and *Peri2F*), we fabricated a series of LSCs containing different concentrations (100, 150, 200, and 250 ppm) that were then cut and polished to obtain 5×5 cm^2 squares with a thickness of 0.3 cm, as suggested by recently published protocols to allow inter-laboratory comparisons [30]. The devices were characterized spectroscopically and their performances were evaluated both in terms of concentration efficiencies and resistance to photodegradation.

2. Experimental section

2.1. Materials

Chemically regenerated methyl methacrylate (r-MMA) was obtained from Madreperla S.p.a. (Milano, Italy). Poly(methyl methacrylate) powder (DIAKON, M_w = 95,000 g/mol) was purchased from Lucite International (Rotterdam, The Netherlands). Azobisisobutyronitrile (AIBN, Sigma Aldrich, USA) was used as an initiator. The syntheses of *Peri2F* and *Nap2Car* are reported elsewhere [26].

2.2. Methods

PMMA free-radical polymerization (FRP) was performed by cell casting [31] pouring a solution of chemically regenerated methyl methacrylate, poly(methyl methacrylate) powder, fluorophore, and initiators into a $12 \times 12 \times 0.3$ cm^3 mold. The molds were composed of two glass sheets separated by a PVC gasket thick, when pressed, as much as the required PMMA sheet. Some metallic clamps allowed the mold to remain sealed during polymerization. The pouring resin (50 g) contains 10 g of DIAKON (20 wt%), 40 g of r-MMA (80 wt%), 0.30 g of AIBN (0.1 wt%). *Nap2Car* and *Peri2F* were added in the desired concentration (100, 150, 200, 250 ppm). The sealed mold was placed in a water-filled tank overnight at a temperature of 50 °C and then it was transferred to an oven for a curing of 4 h reaching 120 °C. At the end of the curing process, the two glass sheets were separated, and the PMMA slab was cut to size by laser cutting and polished.

UV–vis spectra were acquired at room temperature with a Cary 5000 Series UV–vis NIR spectrophotometer (Agilent Technologies, USA). Fluorescence spectra on polymer films were measured at room temperature with a Jobin–Yvon Fluorolog®-3 spectrofluorometer (Horiba, Japan) equipped with a 450 W Xenon arc lamp and double-grating excitation and single-grating emission monochromators.

Photoluminescence quantum yields (PLQY) were determined using a 152 mm diameter Quanta-ϕ integrating sphere (Horiba, Japan). Epifluorescence micrographs were taken on an LED epifluorescence microscope (Schaefer South-East Europe) equipped with LED blue and green 5W light sources and a DeltaPix Invenio 2EIII camera (DeltaPix).

LSC photonic efficiencies were calculated from irradiance spectra acquired using a solar simulator LCS-100 94011A (S/N: 322, AM 1.5G std filter: 69 mW/cm^2 at 254 mm, Oriel Instruments, USA) as the light source and a spectroradiometer connected to an integration sphere provided by Cicci Research s.r.l. (Grosseto, Italy) as the detector. The incident light irradiance spectrum was integrated in the 350–1100 nm range. The absorbed irradiance spectrum was only integrated in correspondence with the absorption peaks, and the edge-emitted irradiance spectrum was integrated from 400 to 800 nm to minimize overestimations of efficiencies due to stray light.

I–V curves for electric device efficiency were obtained by coupling the device with two silicon PV cells (IXOLAR KXOB25-12X1F solar cell 20.0 × 5.65 mm^2, V_{oc} = 0.69 V, I_{sc} = 46.7 mA, FF > 70%, η = 25%, Anysolar Ltd., South Korea) in series, connected to a B2901A precision source/measure unit (Keysight Technologies, USA). The PV cell is masked with black tape to match the LSC edge (50×3 mm^2), limiting the stray light to negligible levels. Silicone grease was used to ensure optical contact between the LSC and the PV cell. The other three edges of the LSC were covered with a reflective aluminum tape. The reported η_{int}, η_{ext}, and η_{dev} [30] values were calculated as the average of three distinct measurements on a $50 \times 50 \times 3$ mm^3 LSC sample. All detailed procedures are reported in the Supplementary Information section.

The accelerated aging test was conducted for 450 min total placing the samples on a controllable hot stage set at 80 °C. The surface temperature of the samples was 70 °C. A LED tower (Cicci research s.r.l., Grosseto, Italy) was used as light source and an optical fiber connected to a spectroradiometer as the detector (CCARK.A.4.Spectroradiometer, Fiber Optic VIS/NIR spectrometer, 2048 pixels, grating VA (360–1100 nm), slit-50, OSC, DCL- UV/VIS), placed at a distance of <1 cm from the polymer sample with a detection angle of ca. 35°. More details are available in the SI.

3. Results and discussion

Peri2F and *Nap2Car* were selected to fabricate $5 \times 5 \times 0.3$ cm^3 r-PMMA slabs according to recent protocols [30,32] and following a widely known industrial procedure [33,34]. Notably, a solution of PMMA (pre-polymer), AIBN (initiator), and fluorophore (at 100, 150, 200, and 250 ppm concentrations) in r-MMA was poured in a glass mold and heated in a water tank overnight to promote the polymerization process. After the curing phase in an oven, the plates were cut and polished. The appearance of the samples is shown in Fig. S2. At first glance, the devices containing *Peri2F* appeared opaque and more colored than their *Nap2Car*-based counterparts; on the contrary, the emission of the latter appeared more intense (Fig. 1a, Fig. S3).

3.1. Spectroscopic investigation

UV–vis absorption and fluorescence investigations were performed to assess any differences in fluorophore features when

dissolved in solution [26] or in PMMA. As shown in Fig. 2, *Nap2Car* displayed an absorption maximum centered at 430 nm, i.e. almost identical to that observed in chloroform solution (434 nm). *Peri2F*, on the other hand, showed a particularly broad absorption peak at 544 nm, close to the 540 nm peak observed in $CHCl_3$ [26]. Notably, *Peri2F* displays a much larger absorption coefficient (ε), responsible for the more intense coloration. This is also evident in $CHCl_3$ solutions, where the ε value for Peri2F stands at 35,500 mol^{-1} L cm^{-1}, notably greater than the 25,600 mol^{-1} L cm^{-1} observed for Nap2Car.

With regard to fluorescence, *Nap2Car* showed a blue-shifted emission compared to the solution (536 nm), with a maximum that shifted with concentration from 499 to 503 nm. The small red shift of the fluorescence maximum with concentration was addressed to the inner filter effect [35] as usually observed for organic fluorophores dispersed in solid polymers [36–38]. The Stokes shift of *Nap2Car* in the r-PMMA slabs was 69–73 nm. Conversely, *Peri2F* displayed an emission peak centered at 602 nm at a concentration of 100 ppm, which shifted progressively to 607 nm at 250 ppm. This agreed with studies in solution, where the emission was centered at 611 nm. *Peri2F* in r-PMMA showed a Stokes shift of 58–63 nm, i.e., slightly lower than that of *Nap2Car*.

Subsequently, we performed quantum yield (QY) measurements aimed at studying the influence of the nature and fluorophore concentration on their emission efficiency. *Nap2Car*, characterized by a QY of 0.77 in solution [26], showed in r-PMMA a decrease from 0.48 to around 0.40 (Fig. 3a) at 100 and 250 ppm pf concentration, respectively. Similarly, *Peri2F*, characterized by a quantum yield of 0.59 in $CHCl_3$ [26], exhibited a comparable trend in r-PMMA at low concentrations (0.60 at 100 ppm), but decreased to 0.49 at 250 ppm. This is a common behavior occurring in fluorophore/polymer dispersions, since an increase in fluorophore concentration makes aggregation-caused quenching (ACQ) effects more likely [7]. Based on the transmittance spectra (Fig. S4), we hypothesized that fluorophore aggregation occurred, leading to damage to the lightguide due to scattering effects and potentially causing emission quenching. Epifluorescent microscopy indeed revealed the formation of micro-sized aggregates of *Peri2F* at 200 and 250 ppm concentrations (see Fig. S5). Conversely, these aggregates were not observed in less concentrated samples or in *Nap2Car*-doped r-PMMA. Although not outstanding nor close to those of the state-of-the-art fluorophores (i.e. Lumogen Red F305, coumarins, and rhodamines, whose high QYs allow the effective use of these dyes in large-scale devices), QYs were still considered interesting for application in LSCs.

3.2. Photonic and electrical efficiencies

Due to its broader, more intense, and more red-shifted absorption, flanked by the higher QY, *Peri2F* appeared the best candidate for LSC applications [39]. By placing an integration sphere on the LSC edge and connected to a calibrated spectroradiometer, one can acquire edge-emission irradiation spectra and integrate them to obtain the total emitted irradiance per unit area. Fig. 3b shows that *Peri2F* produces a much more intense edge emission than *Nap2Car* at 100 ppm; however, the emission intensities are similar at 250 ppm. Since, as mentioned above, the QYs of both fluorophores decrease similarly with increasing concentration, the significant drop in edge-emitted intensity observed for 250 ppm *Peri2F* LSC must be due to phenomena occurring within the optical path. Analyzing the edge-emission spectra (Fig. 3b) and comparing them to the upper surface emission (Fig. 2), we noted that a longer average optical path in the lightguide caused a considerably greater

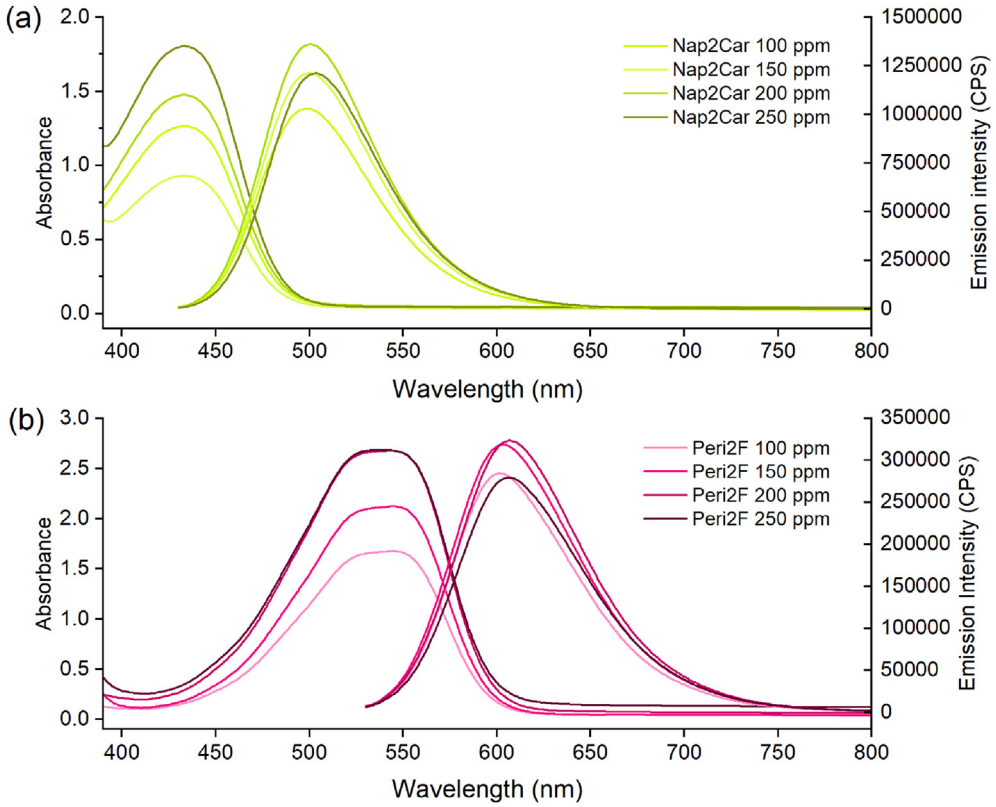

Fig. 2. Absorption (left) and emission (right) spectra of a) Nap2Car and b) Peri2F fluorophores in r-PMMA LSC devices investigated in this study. In the case of Peri2F, samples at 200 and 250 ppm showed coincident spectra due to too low transmittance (thickness = 3 mm).

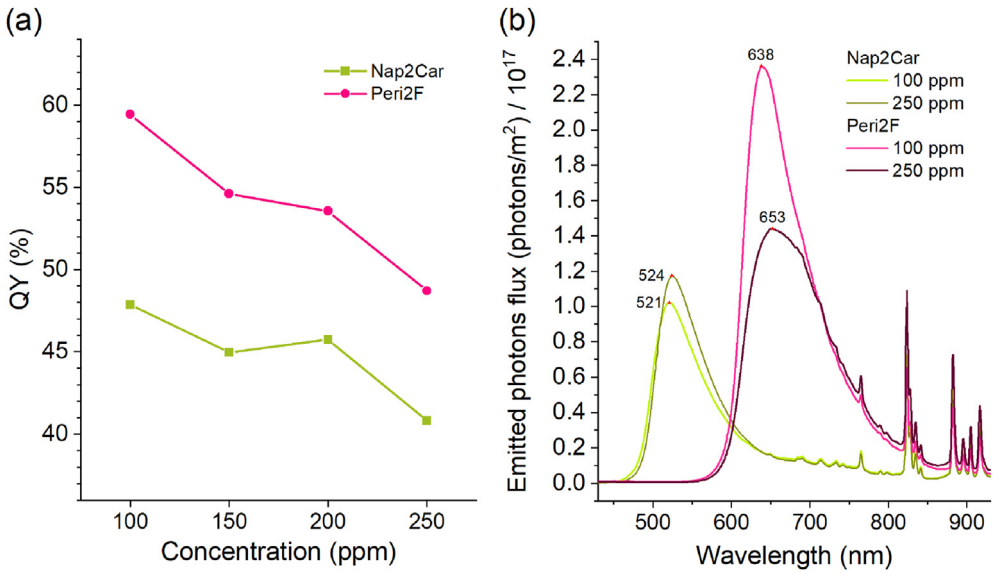

Fig. 3. (a) Photoluminescence quantum yield (QY) of Nap2Car (green) and Peri2F (magenta) in r-PMMA; (b) Edge-emission spectrum of the LSC containing Nap2Car (green) and Peri2F (magenta). The emission maxima of the 100 ppm and 250 ppm concentrations are labeled to show the red shift due to reabsorption effects.

red-shift of the emission peak. For instance, in the case of the LSC containing *Peri2F* at the concentration of 250 ppm, a broad edge emission at 653 nm occurred, with a 46 nm red-shift relative to the peak of the surface emission. This shift is less evident for *Nap2Car*, measuring 21 nm (503–524 nm). This behavior is typically observed in the case of fluorophores with high tendency to reabsorption, which also causes high photon losses and a detrimental effect on the edge-emission intensity [40].

From the edge-emitted irradiance spectrum, it is possible to calculate the number of edge-emitted photons and compare it to that of incident photons to obtain the external photonic efficiency, η_{ext} (Fig. 4a; a more detailed analysis of η_{ext} and the other parameters employed to characterize the performances of the LSC can be found in the SI). As expected, η_{ext} of the *Peri2F*-based LSC remained about twice that of *Nap2Car* over the entire concentration range but was characterized by a significant drop when increasing the concentration, i.e., from 5.7% to 4.4% on going from 100 to 250 ppm. This is probably related to the aggregation of the dye in the r-PMMA matrix even at relatively low concentrations. *Nap2Car*, on the other hand, displayed an η_{ext} below 3% but remained roughly constant on going from 100 to 250 ppm.

To better characterize these phenomena, one can calculate the internal quantum efficiency, η_{int}, by dividing the number of edge-emitted photons by the absorbed photons (Fig. 4b). Surprisingly, in this case, the *Nap2Car* containing-LSC performed about 8% better than *Peri2F*. This result indicates that, despite its higher QY, *Peri2F* appeared to be less effective in re-emitting the absorbed photons, possibly due to higher reabsorption as well as the ACQ effect. Reabsorption may not be relevant in QY determinations, using a small fragment as a sample; however, in a lightguide, characterized by a longer optical path for emitted photons, this effect has a greater impact on efficiency.

To better understand the influence of reabsorption and scattering losses, we measured how the edge-emitted irradiance of the LSCs varied when illuminated with a laser in different positions (laser source wavelength = 405 nm; spot diameter = 1 mm; Fig. S6). As the spot was moved farther from the detector, the optical path length increased, thus the normalized edge irradiance

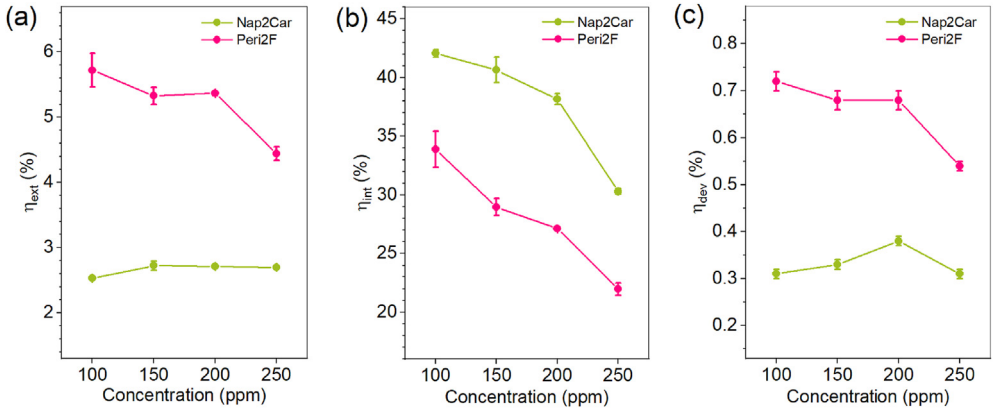

Fig. 4. (a) External photonic efficiency (η_{ext}) of LSCs containing Nap2Car and Peri2F; (b) Internal photonic efficiency (η_{int}) of LSCs containing Nap2Car (green) and Peri2F (magenta); (c) Electrical device efficiency (η_{dev}) of LSCs containing Nap2Car and Peri2F.

was more dependent on the nature and concentration of the fluorophore. At higher *Peri2F* concentrations, we observed that the edge-emitted irradiance appeared to decrease more markedly (Fig. S7). This behavior highlights the tendency of *Peri2F* to reabsorption, given its higher absorption coefficient and a greater spectral overlap of absorption and emission. Conversely, the behavior of *Nap2Car* samples was independent of concentration.

Finally, we measured the electrical device efficiency (η_{dev}) from the edge output power of the LSC coupled to a silicon PV cell and the incident optical power. A solar simulator was used as the light source to replicate outdoor illumination. As shown in Fig. 3d, *Peri2F* containing-LSCs were more effective for energy production, with the highest η_{dev} over 0.7%. *Nap2Car*, on the contrary, endowed r-PMMA LSCs with efficiencies of 0.4% maximum. *Peri2F* can thus be considered the best emitter for LSC technologies among the heptagonal-embedded PADIs investigated, achieving more than half of the performance of a similarly prepared device employing the state-of-the-art lumophore LR305 (η_{dev} = 1.3%) [29].

3.3. Photodegradation studies

In the context of the energy transition and the analysis of the production impact on the overall device performances, it is imperative that LSCs possess robust UV resistance, a characteristic often overlooked in existing literature which can, however, drastically hamper scale-up and technology diffusion. For this purpose, we conducted a photodegradation study to assess the long-term stability of the LSC in a simulated real-life application. The literature details several aging methods, which generally allow to calculate acceleration factors originating from thermal or high irradiation power conditions [41–45]. This study follows an experimental procedure outlined previously based on an ASTM protocol [46] and corresponds to a 4-month outdoor experiment [29]. In this study, an optical fiber was positioned on a hotplate near an LSC fragment under a UV light source to simulate the UV irradiance of radiation corresponding to 1 Sun, and the emission intensity was recorded over time during irradiation. The temperature was set to 80 °C, to reach 70 °C on the upper surface of the device and ensure adequate accelerated aging (details available in the SI). The selected LSCs for this experiment were r-PMMA-*Peri2F* 100 ppm and r-PMMA-*Nap2Car* 200 ppm, which were the best-performing devices of the two series. Remarkably, as shown in Fig. 5, *Peri2F* containing-LSCs maintained a constant emission after 180 simulated hours of direct illumination. *Nap2Car*, on the other hand, degraded quickly, losing roughly 30% over the same timeframe. Hence, there is another reason to prefer *Peri2F* to *Nap2Car* for LSC applications. Moreover, the test on an LSC comprising *Peri2F* and r-PMMA was repeated for a longer time, corresponding to 2900 h of simulated aging. The sample maintained about 100% of the initial emission intensity, with reproducible results across the two datasets (Fig. S8). Assuming a constant degradation rate from the longer test [29], it would take 27,000 h of direct illumination to half its emission intensity (approximately 12.5 years, considering a day consisting of an average of 6 h at 1 Sun irradiation) [47,48]. This is even more remarkable as the impurities present in r-PMMA (e.g., methyl isobutyrate), originating from the depolymerization process, have been shown to increase the rate of photodegradation of fluorophore/PMMA systems [19,29,49–51]. Aware of the variety of photodegradation tests carried out in the literature and the difficulty of comparing them, a test was designed in the harshest conditions we could achieve. We set Far UV, UV, Deep Blue, and Green LED lights at the maximum power (total irradiance = 360 W/m^2, Fig. S9) to irradiate a Peri2F 100 ppm sample at 70 °C. As shown in Fig. S10, the emission irradiance decreased to 98% over 40 testing hours, demonstrating the remarkable photostability of Peri2F in r-PMMA even under the most severe conditions. Moreover, the UV range below 350 nm has been investigated separately, as it was not covered by the LED tower used in the above-mentioned tests. We exposed an LSC fragment to the light of a 400 W high-pressure mercury lamp, whose spectrum has strong emission in the 250–350 nm range (Fig. S11). Overheating of the lamp during operation caused the temperature of the sample to rise to 60 °C, thereby accelerating photodegradation. The QY after 12 h was acquired and was almost unchanged with a slight decrease from 59 to 57% (Fig. S12).

To better highlight the superior performance of the system described here, we compared it to a similar device realized employing the state-of-the-art fluorophore, LR305. Although the latter had a higher initial performance in terms of η_{ext}, under the same photodegradation conditions showed a faster performance

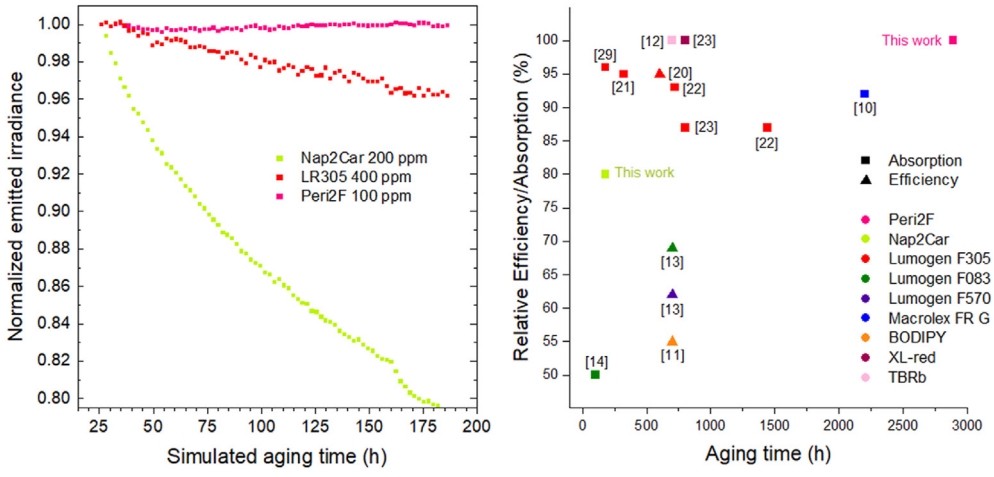

Fig. 5. (a) Normalized emission irradiance of the samples containing Nap2Car (green, 200 ppm), Peri2F (magenta, 100 ppm), and LR305 (red, 400 ppm) over simulated aging time; (b) Photodegradation comparison of the devices presented in this work (Peri2F 100 ppm, Nap2Car 200 ppm) with literature references (indicated between square brackets). The various fluorophores are represented with different colors, which are displayed in the legend. Hollow squares correspond to LSC made from polymers different from acrylics, thus considered less relevant for comparisons. The quantity on the y axis is efficiency (squares) or absorption (triangles) after the aging time (x axis) relative to the pristine samples. It was noted that even a small drop in absorption causes a greater relative decrease in efficiency [14]. More details on the characterization setups are shown in the SI (Table S1).

loss, about 4% in only 180 h of simulated aging [29], in line with what was observed by other groups previously [20–23]. The mechanism of LR305 photodegradation has already been investigated in literature [25]; in particular, it involves the formation of radicals from the homolytic cleavage of the imide C–N bonds (resulting in a phenyl radical) and C–O bonds on phenolic substituents in the bay positions. The formation of these aromatic radicals is favored by delocalization. Similarly, we can argue that for *Nap2Car* the connections between the carbazole units and the aromatic core can degrade by a comparable mechanism, exacerbated by the improved stability of the radicals formed in this case. In addition, a through-space photoinduced electron transfer from the carbazole unit to the naphthalene dicarboximide could initiate a photo-oxidation process leading to an irreversible degradation [52]. On the other hand, in *Peri2F*, the alkyl substituent on the imide group and the presence of fluorine atoms as withdrawing moieties on the dibenzoheptagonal group, which undergo abstraction and photoinduced electron transfer much less easily [53], improve significantly the photostability of this compound. This fact is well reported in the literature and is related to the strong C–F bond and the large electronegativity of fluorine [54,55]. From the results reported in Fig. 5 and in Fig. S8, considering the initial η_{ext} of both systems and their respective degradation rates, we can envisage that an LSC containing *Peri2F* would outperform an identical device containing LR305 during its lifetime. The noticeable superior photostability of *Peri2F* highlights how this system could be an optimal candidate for the fabrication of large-scale sustainable LSCs capable of combining the reduced fabrication impact offered by r-PMMA over the use of virgin materials (a reduction in Global Warming Potential of about 75%) [29] and the extended lifetime provided by *Peri2F*, which prevents the need of replacing LSC panels every few years.

4. Conclusion

In this study, we tested the performances of two different push-pull dyes comprising distorted heptagonal inclusions, i.e., *Peri2F* and *Nap2Car*, as organic fluorophores for bulk 5 × 5 × 0.3 cm^3 LSCs at different concentrations, from 100 ppm to 250 ppm. The cell casting synthesis of PMMA from the regenerated monomer (r-PMMA) resulted in transparent devices with few defects and brightly illuminated edges. The use of chemically regenerated monomer instead of virgin one to produce PMMA slabs has a Global Warming Potential about four times smaller, making the large-scale fabrication of LSC significantly more sustainable and possibly circular. However, the impurities inherently present in the recycled monomer reduce the lifetime of the fluorophores in the final device [29].

Between the two different dyes, *Peri2F* showed a more intense absorption at wavelengths that are more suitable for sunlight harvesting, and a higher quantum yield (more than 50% across the entire range of concentrations tested) which can be considered adequate for LSC applications. As a result, when considering the edge-emission features that characterize the LSC functioning, *Peri2F* displayed a higher η_{ext}, achieving a maximum of 5.7% at 100 ppm concentration. We found that significant reabsorption and aggregation-caused quenching, especially at higher concentrations, limited the performance of the system. Conversely, *Nap2Car*, despite showing lower reabsorption effect and, consequently, a larger η_{int} (above 40%), the η_{ext} was found below 3% in the entire concentration range, demonstrating its poor suitability for LSC applications.

The *Peri2F*/r-PMMA system resulted in an η_{dev} of 0.7%, about half that of LSCs doped by the state-of-the-art fluorophore LR305 and with similar geometrical characteristics. Remarkably, however, when compared to the latter, *Peri2F* showed an outstanding resistance to photodegradation. To the best of our knowledge, no other fluorophore has demonstrated comparable longevity in PMMA matrices. We related this behavior to the structural characteristics of *Peri2F* which present fewer bonds that are susceptible to homolytic cleavage to form stabilized aromatic radicals. Since these devices must have a life of several years in order to be cost-effective and genuinely sustainable, *Peri2F* may be a valid term of comparison among organic emitters for long-lasting LSC installations and could provide novel design rules for the preparation of organic fluorophores that combine suitable optical properties and good photostability.

CRediT authorship contribution statement

Alberto Picchi: Writing – original draft, Methodology, Formal analysis, Data curation. **Kritchasorn Kantarod:** Methodology, Investigation. **Massimo Ilarioni:** Supervision, Methodology. **Marco Carlotti:** Writing – review & editing, Validation, Supervision, Data curation, Conceptualization. **Pawaret Leowanawat:** Supervision. **Andrea Pucci:** Writing – review & editing, Validation, Supervision, Project administration, Funding acquisition.

Declaration of competing interest

The authors declare the following financial interests/personal relationships which may be considered as potential competing interests: Andrea Pucci reports financial support was provided by Ministry of Education and Merit. If there are other authors, they declare that they have no known competing financial interests or personal relationships that could have appeared to influence the work reported in this paper.

Data availability

Data will be made available on request.

Acknowledgments

The authors are grateful to I&S s.r.l. for the opportunity to carry out production at their facilities using their own resources and methods. This research is supported by MUR PRIN 2022 2022ZZC2HZ project “LUminescent Solar Concentrators based on recycled methyl methacrylate and Eco-compatible materials” – LUCE” and PON 2014–2020 “Research and Innovation” resources – Green/Innovation Action – DM MUR 1061/2022.

Appendix A. Supplementary data

Supplementary data to this article can be found online at https://doi.org/10.1016/j.mtener.2024.101646.

References

[1] J. Roncali, Luminescent solar collectors: Quo Vadis? Adv. Energy Mater. 10 (2020) 2001907. https://doi.org/10.1002/aenm.202001907.
[2] P. Bernardoni, G. Mangherini, M. Gjestila, A. Andreoli, D. Vincenzi, Performance optimization of luminescent solar concentrators under several shading conditions, Energies 14 (2021), https://doi.org/10.3390/en14040816.
[3] V. Muteri, F. Guarino, S. Longo, L. Bua, M. Cellura, D. Testa, M. Bonzi, An innovative photovoltaic luminescent solar concentrator window: energy and environmental aspects, Sustain. Times 14 (2022) 1–31, https://doi.org/10.3390/su14074292.
[4] B.S. Richards, I.A. Howard, Luminescent solar concentrators for building integrated photovoltaics: opportunities and challenges, Energy Environ. Sci. 16 (2023) 3214–3239, https://doi.org/10.1039/D3EE00331K.
[5] C. Tummeltshammer, A. Taylor, A.J. Kenyon, I. Papakonstantinou, Losses in luminescent solar concentrators unveiled, Sol. Energy Mater. Sol. Cells 144 (2016) 40–47, https://doi.org/10.1016/j.solmat.2015.08.008.

[6] C. Ceriani, F. Corsini, G. Mattioli, S. Mattiello, D. Testa, R. Po, C. Botta, G. Griffini, L. Beverina, Sustainable by design, large Stokes shift benzothiadiazole derivatives for efficient luminescent solar concentrators, J. Mater. Chem. C 9 (2021) 14815–14826, https://doi.org/10.1039/d1tc03536c.

[7] G. Lyu, J. Kendall, I. Meazzini, E. Preis, S. Bayseç, U. Scherf, S. Clément, R.C. Evans, Luminescent solar concentrators based on energy transfer from an aggregation-induced emitter conjugated polymer, ACS Appl. Polym. Mater. 1 (2019) 3039–3047, https://doi.org/10.1021/acsapm.9b00718.

[8] A.P. Demchenko, Photobleaching of organic fluorophores: quantitative characterization, mechanisms, protection, Methods Appl. Fluoresc. 8 (2020), https://doi.org/10.1088/2050-6120/ab7365.

[9] A. Dubois, M. Canva, A. Brun, F. Chaput, J.P. Boilot, Enhanced photostability of dye molecules trapped in solid xerogel matrices, Synth. Met. 81 (1996) 305–308, https://doi.org/10.1016/S0379-6779(97)80036-7.

[10] S.M. El-Bashir, F.F. Al-Harbi, H. Elburaih, F. Al-Faifi, I.S. Yahia, Red photoluminescent PMMA nanohybrid films for modifying the spectral distribution of solar radiation inside greenhouses, Renew. Energy 85 (2016) 928–938, https://doi.org/10.1016/j.renene.2015.07.031.

[11] A.M. Mooney, K.E. Warner, P.J. Fontecchio, Y.Z. Zhang, B.P. Wittmershaus, Photodegradation in multiple-dye luminescent solar concentrators, J. Lumin. 143 (2013) 469–472, https://doi.org/10.1016/j.jlumin.2013.05.029.

[12] Y. Zhang, Z. Zheng, Z. Gan, R. Huang, X. Zhang, Engineering highly emissive tetra(t-butyl)rubrene/off-stoichiometry thiol-ene hybrids toward flexible luminescent solar concentrator-integrated photovoltaics with excellent stability, Small Sci 2400121 (2024) 1–9, https://doi.org/10.1002/smsc.202400121.

[13] R. Kinderman, L.H. Slooff, A.R. Burgers, N.J. Bakker, A. Büchtemann, R. Danz, J.A.M. van Roosmalen, I-V performance and stability study of dyes for luminescent plate concentrators, J. Sol. Energy Eng. 129 (2007) 277–282, https://doi.org/10.1115/1.2737469.

[14] A.A. Earp, J.B. Franklin, G.B. Smith, Absorption tails and extinction in luminescent solar concentrators, Sol. Energy Mater. Sol. Cells 95 (2011) 1157–1162, https://doi.org/10.1016/j.solmat.2010.12.044.

[15] T. Dienel, C. Bauer, I. Dolamic, D. Brühwiler Dominik, Spectral-based analysis of thin film luminescent solar concentrators, Sol. Energy 84 (2010) 1366–1369, https://doi.org/10.1016/j.solener.2010.04.015.

[16] C. Papucci, R. Charaf, C. Coppola, A. Sinicropi, M. Di Donato, M. Taddei, P. Foggi, A. Battisti, B. De Jong, L. Zani, A. Mordini, A. Pucci, M. Calamante, G. Reginato, Luminescent solar concentrators with outstanding optical properties by employment of D-A-D quinoxaline fluorophores, J. Mater. Chem. C 9 (2021) 15608–15621, https://doi.org/10.1039/d1tc02923a.

[17] C. Papucci, A. Dessì, C. Coppola, A. Sinicropi, G. Santi, M. Di Donato, M. Taddei, P. Foggi, L. Zani, G. Reginato, A. Pucci, M. Calamante, A. Mordini, Benzo[1,2-d:4,5-d′]bisthiazole fluorophores for luminescent solar concentrators: synthesis, optical properties and effect of the polymer matrix on the device performances, Dyes Pigments 188 (2021) 109207, https://doi.org/10.1016/j.dyepig.2021.109207.

[18] M. Carlotti, G. Ruggeri, F. Bellina, A. Pucci, Enhancing optical efficiency of thin-film luminescent solar concentrators by combining energy transfer and stacked design, J. Lumin. 171 (2016) 215–220, https://doi.org/10.1016/j.jlumin.2015.11.010.

[19] A.A. Earp, T. Rawling, J.B. Franklin, G.B. Smith, Perylene dye photodegradation due to ketones and singlet oxygen, Dyes Pigments 84 (2010) 59–61, https://doi.org/10.1016/j.dyepig.2009.06.012.

[20] M.G. Hyldahl, S.T. Bailey, B.P. Wittmershaus, Photo-stability and performance of CdSe/ZnS quantum dots in luminescent solar concentrators, Sol. Energy 83 (2009) 566–573, https://doi.org/10.1016/j.solener.2008.10.001.

[21] Y. Li, Y. Sun, Y. Zhang, W.J. Dong, Improving the photostability of printed organic photovoltaics through luminescent solar concentrators, Opt. Mater. 108 (2020) 110194, https://doi.org/10.1016/j.optmat.2020.110194.

[22] J.M. Delgado-Sanchez, Luminescent solar concentrators: photo-stability analysis and long-term perspectives, Sol. Energy Mater. Sol. Cells 202 (2019) 110134, https://doi.org/10.1016/j.solmat.2019.110134.

[23] D. Pintossi, A. Colombo, M. Levi, C. Dragonetti, S. Turri, G. Griffini, UV-curable fluoropolymers crosslinked with functional fluorescent dyes: the way to multifunctional thin-film luminescent solar concentrators, J. Mater. Chem. A 5 (2017) 9067–9075, https://doi.org/10.1039/C7TA01692A.

[24] I. Baumberg, O. Berezin, A. Drabkin, B. Gorelik, L. Kogan, M. Voskobojnik, M. Zaidman, Effect of polymer matrix on photo-stability of photo-luminescent dyes in multi-layer polymeric structures, Polym. Degrad. Stabil. 73 (2001) 403–410, https://doi.org/10.1016/S0141-3910(01)00119-7.

[25] G. Griffini, L. Brambilla, M. Levi, M. Del Zoppo, S. Turri, Photo-degradation of a perylene-based organic luminescent solar concentrator: molecular aspects and device implications, Sol. Energy Mater. Sol. Cells 111 (2013) 41–48, https://doi.org/10.1016/j.solmat.2012.12.021.

[26] K. Kantarod, D. Soorukram, C. Kuhakarn, P. Surawatanawong, W. Wattanathana, V. Reutrakul, P. Leowanawat, Color-tunable emissive heptagon-embedded polycyclic aromatic dicarboximides, Chem. Commun. 58 (2022) 9468–9471, https://doi.org/10.1039/d2cc03461a.

[27] G. Griffini, Host matrix materials for luminescent solar concentrators: recent achievements and forthcoming challenges, Front. Mater. 6 (2019) 1–8, https://doi.org/10.3389/fmats.2019.00029.

[28] Y. Li, X. Zhang, Y. Zhang, R. Dong, C.K. Luscombe, Review on the role of polymers in luminescent solar concentrators, J. Polym. Sci. Part A Polym. Chem. 57 (2019) 201–215, https://doi.org/10.1002/pola.29192.

[29] A. Picchi, I. Bettini, M. Ilarioni, M. Carlotti, A. Pucci, Assessing the performance of sustainable luminescent solar concentrators based on chemically recycled poly(methyl methacrylate), RSC Appl. Polym. (2024), https://doi.org/10.1039/D4LP00067F.

[30] M.G. Debije, R.C. Evans, G. Griffini, Laboratory protocols for measuring and reporting the performance of luminescent solar concentrators, Energy Environ. Sci. 14 (2021) 293–301, https://doi.org/10.1039/d0ee02967j.

[31] G. Ittmann, Patent Application Publication US 2006/0237872 A1, U.S. Patent US2006/0237872 A1, 2006. https://patentimages.storage.googleapis.com/dd/04/e6/ae97831ad8b169/US20060237872A1.pdf.

[32] C. Yang, H.A. Atwater, M.A. Baldo, D. Baran, C.J. Barile, M.C. Barr, M. Bates, M.G. Bawendi, M.R. Bergren, B. Borhan, C.J. Brabec, S. Brovelli, V. Bulović, P. Ceroni, M.G. Debije, J.-M. Delgado-Sanchez, W.-J. Dong, P.M. Duxbury, R.C. Evans, S.R. Forrest, D.R. Gamelin, N.C. Giebink, X. Gong, G. Griffini, F. Guo, C.K. Herrera, A.W.Y. Ho-Baillie, R.J. Holmes, S.-K. Hong, T. Kirchartz, B.G. Levine, H. Li, Y. Li, D. Liu, M.A. Loi, C.K. Luscombe, N.S. Makarov, F. Mateen, R. Mazzaro, H. McDaniel, M.D. McGehee, F. Meinardi, A. Menéndez-Velázquez, J. Min, D.B. Mitzi, M. Moemeni, J.H. Moon, A. Nattestad, M.K. Nazeeruddin, A.F. Nogueira, U.W. Paetzold, D.L. Patrick, A. Pucci, B.P. Rand, E. Reichmanis, B.S. Richards, J. Roncali, F. Rosei, T.W. Schmidt, F. So, C.-C. Tu, A. Vahdani, W.G.J.H.M. van Sark, R. Verduzco, A. Vomiero, W.W.H. Wong, K. Wu, H.-L. Yip, X. Zhang, H. Zhao, R.R. Lunt, Consensus statement: standardized reporting of power-producing luminescent solar concentrator performance, Joule 6 (2022) 8–15, https://doi.org/10.1016/j.joule.2021.12.004.

[33] P. Gerard, D. Callin, A Liquid (Meth)acrylic Syrup, its Method of Polymerization, Use and Molted Article Obtained Thereof, 2016. Patent US 2016/0271610.

[34] K. Charmondusit, L. Seeluangsawat, Recycling of poly(methyl methacrylate) scrap in the styrene-methyl methacrylate copolymer cast sheet process, Resour. Conserv. Recycl. 54 (2009) 97–103, https://doi.org/10.1016/j.resconrec.2009.07.005.

[35] S. Kumar Panigrahi, A. Kumar Mishra, Inner filter effect in fluorescence spectroscopy: as a problem and as a solution, J. Photochem. Photobiol. C Photochem. Rev. 41 (2019) 100318, https://doi.org/10.1016/j.jphotochemrev.2019.100318.

[36] E. Rosadoni, F. Bellina, M. Lessi, C. Micheletti, F. Ventura, A. Pucci, Y-shaped alkynylimidazoles as effective push-pull fluorescent dyes for luminescent solar concentrators (LSCs), Dyes Pigments 201 (2022), https://doi.org/10.1016/j.dyepig.2022.110262.

[37] C. Micheletti, Q. Wang, F. Ventura, M. Turelli, I. Ciofini, C. Adamo, A. Pucci, Red-emitting tetraphenylethylene derivative with aggregation-induced enhanced emission for luminescent solar concentrators: a combined experimental and density functional theory study, Aggregate 3 (2022) 1–10, https://doi.org/10.1002/agt2.188.

[38] M. Bartolini, C. Micheletti, A. Picchi, C. Coppola, A. Sinicropi, M. Di Donato, P. Foggi, A. Mordini, G. Reginato, A. Pucci, L. Zani, M. Calamante, Orange/red benzo[1,2- b :4,5- b ′]dithiophene 1,1,5,5-tetraoxide-based emitters for luminescent solar concentrators: effect of structures on fluorescence properties and device performances, ACS Appl. Energy Mater. 6 (2023) 4862–4880, https://doi.org/10.1021/acsaem.3c00362.

[39] M.G. Debije, P.P.C. Verbunt, Thirty years of luminescent solar concentrator research: solar energy for the built environment, Adv. Energy Mater. 2 (2012) 12–35, https://doi.org/10.1002/aenm.201100554.

[40] O.M. ten Kate, K.M. Hooning, E. van der Kolk, Quantifying self-absorption losses in luminescent solar concentrators, Appl. Opt. 53 (2014) 5238, https://doi.org/10.1364/ao.53.005238.

[41] K. Wu, H. Li, V.I. Klimov, Tandem luminescent solar concentrators based on engineered quantum dots, Nat. Photonics 12 (2018) 105–110, https://doi.org/10.1038/s41566-017-0070-7.

[42] H. Zhao, G. Liu, S. You, F.V.A. Camargo, M. Zavelani-Rossi, X. Wang, C. Sun, B. Liu, Y. Zhang, G. Han, A. Vomiero, X. Gong, Gram-scale synthesis of carbon quantum dots with a large Stokes shift for the fabrication of eco-friendly and high-efficiency luminescent solar concentrators, Energy Environ. Sci. 14 (2021) 396–406, https://doi.org/10.1039/d0ee02235g.

[43] W. Li, X. Wang, J. Lin, X. Meng, L. Wang, M. Wang, Q. Jing, Y. Song, A. Vomiero, H. Zhao, Controllable and large-scale synthesis of carbon quantum dots for efficient solid-state optical devices, Nano Energy 122 (2024) 109289, https://doi.org/10.1016/j.nanoen.2024.109289.

[44] F. Corsini, E. Tatsi, A. Colombo, C. Dragonetti, C. Botta, S. Turri, G. Griffini, Highly emissive fluorescent silica-based core/shell nanoparticles for efficient and stable luminescent solar concentrators, Nano Energy 80 (2021) 105551, https://doi.org/10.1016/j.nanoen.2020.105551.

[45] J.S. Batchelder, A.H. Zewai, T. Cole, Luminescent solar concentrators 1: theory of operation and techniques for performance evaluation, Appl. Opt. 18 (1979) 3090, https://doi.org/10.1364/AO.18.003090.

[46] Standard guide for accelerated aging of sterile medical device packages 1 11, ASTM F1980-02, 2002, pp. 1–6.

[47] M.P. Sammartino, M. Castrucci, D. Ruiu, G. Visco, L. Campanella, Photostability and toxicity of finasteride, diclofenac and naproxen under simulating sunlight exposure: evaluation of the toxicity trend and of the packaging photoprotection, Chem. Cent. J. 7 (2013) 181, https://doi.org/10.1186/1752-153X-7-181.

[48] A.F. Mansour, Optical efficiency and optical properties of luminescent solar concentrators, Polym. Test. 17 (1998) 333–343, https://doi.org/10.1016/S0142-9418(97)00061-5.

[49] G. Seybold, G. Wagenblast, New perylene and violanthrone dyestuffs for fluorescent collectors, Dyes Pigments 11 (1989) 303–317, https://doi.org/10.1016/0143-7208(89)85048-X.

[50] J. Kowalonek, H. Kaczmarek, M. Kurzawa, Effect of UV-irradiation on fluorescence of poly(methyl methacrylate) films with photosensitive organic compounds, J. Photochem. Photobiol. Chem. 319–320 (2016) 18–24, https://doi.org/10.1016/j.jphotochem.2015.12.017.
[51] M. Plouzeau, S. Piogé, F. Peilleron, L. Fontaine, S. Pascual, Polymer/dye blends: preparation and optical performance: a short review, J. Appl. Polym. Sci. 139 (2022) 1–16, https://doi.org/10.1002/app.52861.
[52] R. Turrisi, A. Sanguineti, M. Sassi, B. Savoie, A. Takai, G.E. Patriarca, M.M. Salamone, R. Ruffo, G. Vaccaro, F. Meinardi, T.J. Marks, A. Facchetti, L. Beverina, Stokes shift/emission efficiency trade-off in donor–acceptor perylenemonoimides for luminescent solar concentrators, J. Mater. Chem. A 3 (2015) 8045–8054, https://doi.org/10.1039/C5TA01134E.
[53] R.C. Evans, P. Douglas, H.D. Burrows, Applied Photochemistry, 2014, https://doi.org/10.1007/978-90-481-3830-2.
[54] G. Yan, Photochemical and electrochemical strategies for hydrodefluorination of fluorinated organic compounds, Chem. Eur J. 28 (2022), https://doi.org/10.1002/chem.202200231.
[55] R.S. Davidson, J.W. Goodin, G. Kemp, The Photochemistry of Aryl Halides and Related Compounds, 1984, pp. 191–233, https://doi.org/10.1016/S0065-3160(08)60149-5.